Journal of Nuclear Materials 490 (2017) 66–74

Contents lists available at ScienceDirect

Journal of Nuclear Materials

journal homepage: www.elsevier.com/locate/jnucmat

Microstructural evolution of pure tungsten neutron irradiated with a mixed energy spectrum☆

Takaaki Koyanagi [a, *], N.A.P. Kiran Kumar [a], Taehyun Hwang [b], Lauren M. Garrison [a], Xunxiang Hu [a], Lance L. Snead [c], Yutai Katoh [a]

[a] Oak Ridge National Laboratory, Oak Ridge, TN 37831, USA
[b] Tohoku University, Sendai, 980-8579, Japan
[c] Massachusetts Institute of Technology, Cambridge, MA 02139, USA

ARTICLE INFO

Article history:
Received 11 January 2017
Received in revised form
16 March 2017
Accepted 10 April 2017
Available online 13 April 2017

ABSTRACT

Microstructures of single-crystal bulk tungsten (W) and polycrystalline W foil with a strong grain texture were investigated using transmission electron microscopy following neutron irradiation at ~90–800 °C to 0.03–4.6 displacements per atom (dpa) in the High Flux Isotope Reactor with a mixed energy spectrum. The dominant irradiation defects were dislocation loops and small clusters at ~90 °C. Additional voids were formed in W irradiated at above 460 °C. Voids and precipitates involving transmutation rhenium and osmium were the dominant defects at more than ~1 dpa. We found a new phenomenon of microstructural evolution in irradiated polycrystalline W: Re- and Os-rich precipitation along grain boundaries. Comparison of results between this study and previous studies using different irradiation facilities revealed that the microstructural evolution of pure W is highly dependent on the neutron energy spectrum in addition to the irradiation temperature and dose.

1. Introduction

The technological feasibility of fusion reactors is strongly dependent on the development of plasma-facing material (PFM) that simultaneously fulfills several requirements, such as efficient heat transfer, ability to withstand off-normal heat loads, limited radioactive tritium retention, and low erosion by particle bombardment. These critical properties requirements make the development of PFM an extremely challenging task. Tungsten (W) materials, including alloys and composites, are the leading candidates because of their inherent high-temperature capability, high thermal conductivity, and low sputtering yield [1,2]. The fusion reaction (d, t) produces 14 MeV neutrons, and the consequences of neutron irradiation of the tungsten components is a great concern in development of W PFM [1,2].

The neutron irradiation response of W and W-based alloys has been investigated intensively to capture the dependence of their microstructures on irradiation temperature, dose, and neutron energy spectrum [3–6]. The microstructural characterization of these irradiated W materials enabled an evaluation of the radiation damage under various irradiation conditions, covering an irradiation temperature range from 300 to 900 °C and a dose range from 0.03 to 1.5 displacements per atom (dpa). The results show that dislocation loops, voids, and transmutation-induced precipitates are the most important irradiation defects and are strongly dependent on the irradiation conditions. Recent studies of neutron irradiation effects on W using material testing reactors found that (1) irradiation hardening of W materials depends strongly on the original composition [7] and neutron spectrum [8,9], and (2) significant hardening of W irradiated in a mixed neutron energy spectrum to >1 dpa is attributable to irradiation-induced precipitation [9]. The source of the precipitation is the alloy elements and transmutation elements, such as rhenium (Re) and osmium (Os)

☆ This manuscript has been authored by UT-Battelle, LLC under Contract No. DE-AC05-00OR22725 with the U.S. Department of Energy. The United States Government retains and the publisher, by accepting the article for publication, acknowledges that the United States Government retains a non-exclusive, paid-up, irrevocable, worldwide license to publish or reproduce the published form of this manuscript, or allow others to do so, for United States Government purposes. The Department of Energy will provide public access to these results of federally sponsored research in accordance with the DOE Public Access Plan (http://energy.gov/downloads/doe-public-access-plan).

* Corresponding author. Current address: Materials Science and Technology Division, Oak Ridge National Laboratory, 1 Bethel Valley Road, Oak Ridge, TN 37831-6140, USA.
E-mail address: koyanagit@ornl.gov (T. Koyanagi).

http://dx.doi.org/10.1016/j.jnucmat.2017.04.010
0022-3115/

[10]. Various researchers have focused on this particularly interesting topic since the 1980s. For instance, Sikka et al. have analyzed the irradiation-induced precipitation in neutron-irradiated W alloys [11]; the precipitation of an α-Mn crystal structure, i.e., χ phase (WRe_3), was found in a W-25 at. % Re alloy following fast neutron irradiation at ~1000 °C with limited production of the transmutation elements. The phase was identified based on analysis of the electron diffraction pattern and W-Re phase diagram. Williams et al. also found the χ phase in W-Re alloys with different compositions irradiated at high temperatures (>900 °C) without significant transmutation [3]. They also found large χ precipitates and unidentified phases associated with the grain boundaries at 1100 and 1500 °C, respectively. Nemoto et al. reported the presence of a needle-shaped σ phase (WRe) with a CrFe structure in addition to a platelet-type χ phase in a W-26 wt % Re alloy irradiated at 373–800 °C in the Fast Flux Test Facility [12]. Although precipitates in W-xRe alloys subjected to neutron irradiation have been observed by several researchers, those studies have not investigated the precipitates in W that originate from transmutation. Identifying the mutual interactions of transmutant elements and radiation-induced damage is more relevant to fusion reactor conditions.

One previous study of transmutation precipitation, completed by Fukuda et al., found precipitates in pure W irradiated in the High Flux Isotope Reactor (HFIR) at Oak Ridge National Laboratory with a mixed spectrum of thermal and fast neutrons [6]. Irradiation-induced precipitation of pure W is known to be caused by the production of transmutation elements of Re and Os [13,14]. Rhenium is produced from W by an (n, γ) reaction with a large reaction cross section with thermal neutrons. Osmium is a secondary transmutation product, resulting from Re. In the Fukuda et al. study, electron diffraction analysis indicated that the precipitates were σ and χ phases.

Despite the knowledge of the irradiation-induced precipitation mentioned, the underlying mechanism of precipitation is still poorly understood with respect to the mutual interactions between transmutant elements and radiation defects. Owing to the lack of a fusion-relevant neutron source, a more systematic summary of the neutron irradiation response of pure W irradiated in a large irradiation temperature and dose range is much needed to inform and verify modeling endeavors to better predict the irradiation behavior of W under fusion reactor conditions. In the present study, we introduce our recent efforts to characterize the microstructures of single-crystalline and polycrystalline pure W irradiated in HFIR with a mixed energy spectrum (~90–800 °C, 0.03–4.6 dpa), providing more insight into microstructure evolution as a function of irradiation temperature and dose. In addition, the underlying mechanisms controlling transmutation-induced precipitation are discussed.

2. Experimental procedure

The single-crystal W used in this study was high-purity material purchased from Goodfellow Co. in Coraopolis, Pennsylvania. SS-J2 type tensile test specimens were machined directly from the procured single-crystalline W rod. The tensile axis was oriented to a [011] or [001] direction. The undeformed tab section of the specimen was used for the microstructural investigation. The chemical composition analysis was performed at Luvak Inc. The major impurities determined using the inert gas fusion technique were 10 ppm O; <10 ppm N; 20 ppm C, <5 ppm S; 3 ppm H, and 140 ppm Cu and N. The carbon and sulfur content were determined using combustion infrared detection; vacuum hot extraction was used to determine the hydrogen content; copper was quantified through direct current plasma emission spectroscopy. The polycrystalline W used was produced by PLANSEE Metall GMbH, Reutte, Austria, by powder sintering and then hot and cold rolling. The specimen dimensions were $16 \times 4 \times 0.1$ mm^3. The rolling direction was parallel to the length direction. The material was 99.97% pure; the major impurity elements included <100 ppm Mo, <30 ppm C, <30 ppm Fe, and <20 ppm O, as guaranteed by the manufacturer. The mechanical properties and microstructure of this foil were evaluated in previous work [15].

The specimens were irradiated to fluences of $0.1–14.1 \times 10^{25}$ n/m^2 [E > 0.1 MeV] in the peripheral target positions (PTPs) or hydraulic tube (HT) facility of the HFIR. A fluence of 1×10^{25} n/m^2 [E > 0.1 MeV] corresponds to ~0.3 dpa in W [16]. In the HT facility, the irradiation was performed in perforated rabbit capsules in which the W specimens were seal-wrapped with an aluminum foil. The foil exterior was in direct contact with the HFIR coolant water (around 60 °C), and the specimen temperature was presumably within 80–100 °C. For convenience, 90 °C is used as the nominal radiation temperature of those specimens. For irradiation in the PTPs, irradiation temperatures were determined using passive thermometry via temperature monitors made of high-purity chemical-vapor–deposited SiC obtained from Rohm and Haas Co. (currently Dow Chemical Co., Marlborough, Massachusetts). The temperature monitors were placed near the W specimens during irradiation. The irradiation temperatures were calculated from recovery of the thermal expansion during continuous dilatometry [17]. Irradiation conditions for each specimen are summarized in Table 1. Only the design irradiation temperature is shown for the polycrystalline specimens because of the unavailability of the temperature monitors. Previous simulation studies showed the production of 5–10 at. % Re and 1–5 at. % Os via atomic transmutation in W irradiated to 1 dpa in the HFIR [6,13].

The microstructures of the specimens were observed using a JEOL JEM2100F transmission electron microscope (TEM) operated at 200 kV. TEM foils were prepared using a focused ion beam system (FEI Quanta 3D 200i Dual Beam) operated at 30 kV for initial milling and at 2–5 kV for final thinning, followed by low-energy ion milling using a Fischione Model 1040 NanoMill operated at 600 and 900 eV. The defect clusters were observed by a weak-beam dark-field (WBDF) technique with a g/3–4 g condition. All the weak-beam micrographs shown in this study were taken with $\boldsymbol{s_g} > 0$. Precipitates were observed by TEM DF imaging using a diffraction spot from the precipitate. Voids were confirmed via through-focus imaging in TEM mode. Chemical analysis was also conducted with an energy-dispersive x-ray spectroscope (EDS) in a scanning transmission electron microscope (STEM). STEM bright-field (BF) and high-angle-annular dark-field (HAADF) imaging were also used to observe voids [18] and precipitates. The foil thickness was evaluated by means of an electron energy loss spectroscopy (EELS) log-ratio technique. Electron backscatter diffraction (EBSD) analysis was carried out using an Oxford Instruments Nordlys-2 detector on a Versa 3D DualBeam scanning electron microscope/focused ion beam. Post-processing of the EBSD data was conducted using an Oxford Instruments Tango software to evaluate grain size and grain boundary misorientation.

3. Results

3.1. Single-crystal tungsten

The unirradiated single-crystal W contained a very limited amount of pre-existing dislocations [16]. Observed irradiation defects included small defect clusters, dislocation loops, voids, and precipitates, depending on the irradiation condition. The sizes and densities of the defects are summarized in Table 1. WBDF images of the single-crystal W unirradiated and irradiated under different

Table 1
Irradiation conditions and summary of microstructures of irradiated W materials.

Specimen	Material Type	Irradiation Temperature [°C]	Fluence [10^{25} n/m^2 (>0.1 MeV)]	Dose [dpa]	Loop Diameter [nm]	Loop Density [$\times 10^{22}$m^{-3}]	Void Diameter [nm]	Loop Density [$\times 10^{22}$m^{-3}]	Precipitate Size [nm]	Precipitate Density [$\times 10^{22}$m^{-3}]
1W25	Single crystal	~90	0.10	0.03	1.4	3.3	–	–	–	–
1W43	Single crystal	~90	1.95	0.6	3.2	7.2	–	–	–	–
1W47	Single crystal	460	0.10	0.03	1.9	4.4	3.9	0.3	–	–
1W53	Single crystal	800	0.46	0.15	2.0	4.8	3.9	0.2	–	–
1W17	Single crystal	710	2.20	0.70	2.2	2.4	4.1	0.3	–	–
1W19	Single crystal	770	9.00	2.88	3.6	3.2	6.3	0.3	Needle type: 37.8 Plate type: 5.8	Needle type: 1.2 Plate type: 0.4
1W158	Polycrystalline	650[a]	7.44	2.4	–	–	5.6	0.4	Needle type: 32.8 Plate type: 17.2	Needle type: 0.6 Plate type: 0.4
1W125	Polycrystalline	500[a]	14.14	4.6	–	–	5.8	0.6	Needle type: 30.5 Plate type: 18.2	Needle type: 1.0 Plate type: 0.7

[a] Design irradiation temperature.

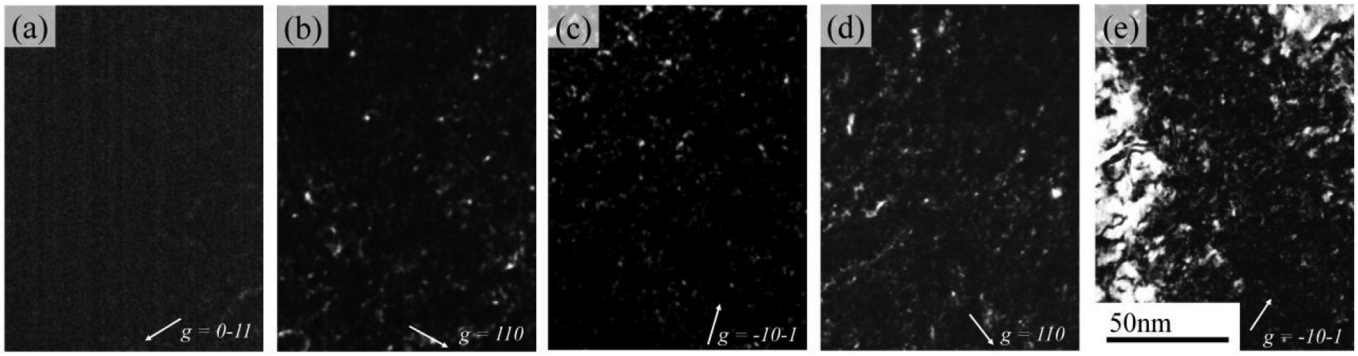

Fig. 1. WBDF micrographs of single-crystal tungsten without irradiation (a) and with neutron irradiation (b) at ~90 °C to 0.6 dpa, (c) at 800 °C to 0.15 dpa, (d) at 710 °C to 0.70 dpa, and (e) at 770 °C to 2.88 dpa. All the images were taken from near [−111] direction. The *g*-vectors are shown as white arrows. The micrographs show formation of defect clusters (white contrast) with a few nm size in average following irradiation.

temperatures and doses are shown in Fig. 1. Note that unirradiated and irradiated specimens were prepared for TEM using the same method (FIB followed by low-energy ion milling). Small defect clusters and loops were observed under all irradiation conditions. The average sizes were a few nanometers, regardless of irradiation temperature and fluence in this study. The number densities were on the order of 1×10^{22} m^{-3} and were also apparently insensitive to the irradiation conditions. These results are consistent with dislocation loop size and densities as observed in pure W specimens ion-irradiated to the same level of displacement damage [19]. The habit plane and Burger's vector of the small defects were not identified because of their small sizes.

Fig. 2 shows voids in irradiated single-crystal W. The lowest irradiation temperature and dose that produced visible voids were 460 °C and 0.03 dpa, respectively (Fig. 2a). The number density of relatively large voids increased with increasing temperature and dose (Fig. 2b and c). The average void diameter was around 5 nm, which was apparently insensitive to the irradiation temperature up to 800 °C. The number density of voids was on the order of 1×10^{21} m^{-3}. Note that only voids with diameters larger than ~1 nm were considered for statistical analysis owing to the limitations of the imaging. Faceted voids with relatively large sizes (diameter > ~10 nm) were observed. The facet orientations are discussed in Section 3.2. Voids were not observed in any single-crystal samples irradiated at ~90 °C.

The precipitates were detectable by TEM DF imaging following irradiation at 770 °C to 2.88 dpa. The DF micrographs taken using diffraction spots attributed to the precipitates revealed two types of precipitates with oval or plate shapes (Fig. 3b) and needle shapes (Fig. 3c). Both types of precipitates were also observed in the pure W material irradiated at the HFIR to a lower dose of 0.98 dpa [6]. Although the DF imaging revealed the presence of at least two types of precipitates, this technique could not capture the overall shapes of the precipitates because of the required the small specimen thickness. The STEM BF micrograph (Fig. 3d) at a relatively thick (60–80 nm) area captured the structure of the precipitation and revealed that the most numerous precipitates were needle shaped.

3.2. Polycrystalline tungsten foil

Fig. 4 shows the results of EBSD analysis of the unirradiated W foil surface. The average grain size (the equivalent circle diameter of the grain) was 3.1 μm. The inverse pole figure map found an anisotropic microstructure in the material; grains with <001> parallel to the surface normal were dominant. The majority of the grains were elongated to a <101> axis, which corresponds to the rolling direction (horizontal direction in the image). The post-EBSD analysis showed that the fraction of low-angle grain boundaries with a misorientation angle of less than 15° was ~70%. The

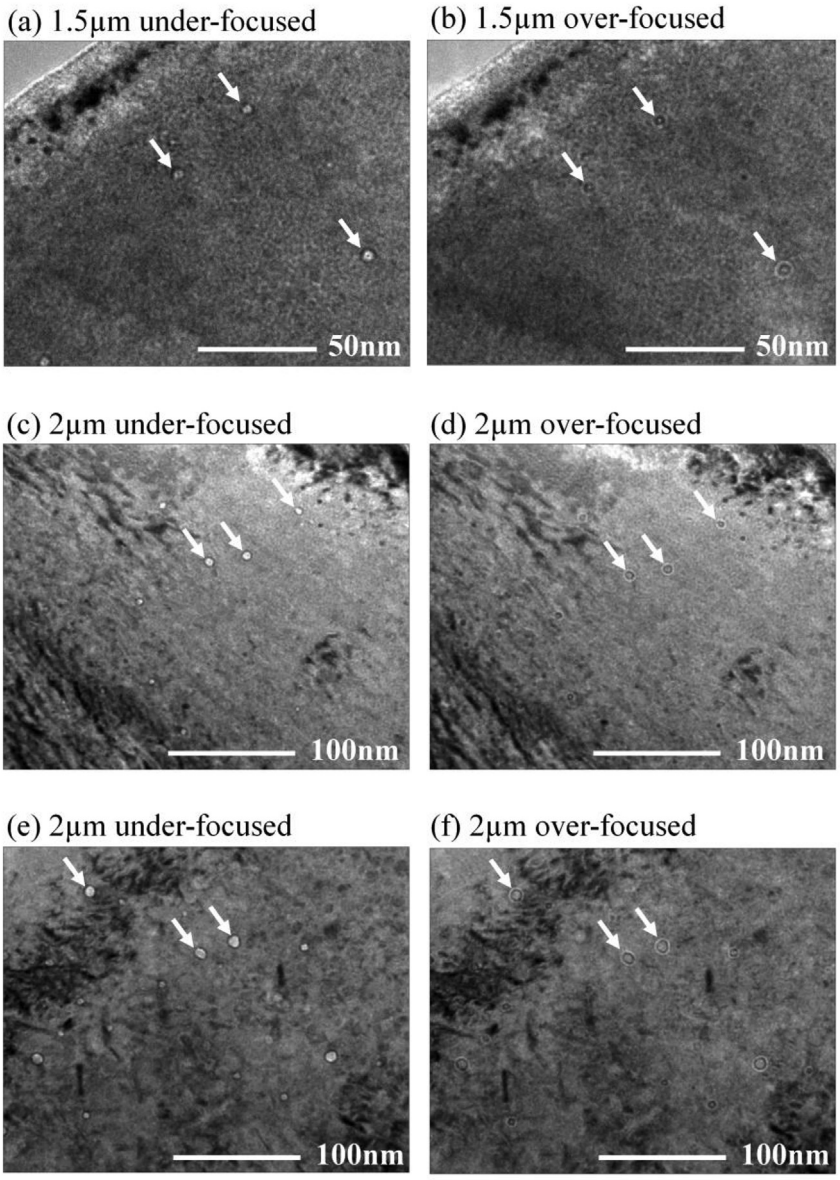

Fig. 2. Voids in irradiated single-crystal tungsten. The irradiation conditions (temperature/dose) are (a, b) 460°C/0.03 dpa, (c, d) 800°C/0.15 dpa, and (e, f) 770°C/2.88 dpa. The voids were confirmed by though-focus imaging. White arrows indicate voids.

observation was consistent with the results of the previous study of a similar W foil by Reiser et al. [15]. Fig. 5 shows cross section TEM micrographs of the unirradiated W foil. The vertical direction in the images corresponds to the foil thickness direction. Most of the grains extended in the horizontal direction. The grain height was typically 200–300 nm. The STEM BF revealed the presence of line dislocations within the grains (Fig. 5, right image).

The polycrystalline W specimens were investigated following relatively high-dose irradiations: 650°C/2.4 dpa and 500°C/4.6 dpa. The dominant irradiation defects were precipitates and voids. Dislocation loops were not clearly observed because the significant precipitation made the imaging difficult, and distinguishing between the precipitates and defect clusters was challenging. The voids and precipitates were observed using STEM techniques, as shown in Fig. 6. The grain boundaries in the material were observed in the STEM-BF image (Fig. 6a), although the image contrast of the voids and precipitates was not strong. The STEM-HAADF image (Fig. 6b) clearly shows voids with darker contrast. The precipitates in Fig. 6b appear slightly brighter because they are Re and/or Os rich and thus have heavier elements than the surrounding W matrix. The voids were distributed within the grains, but no voids existed on the grain boundaries. The needle-type precipitates were dominant in the STEM-HAADF micrograph. An interesting finding is that the voids and precipitates appeared to exist in close proximity, and few voids were observed in the area where the needle-shaped precipitates were absent.

TEM imaging at higher magnification captured the voids and precipitates (Fig. 7). Voids with sizes of ~10 nm or larger were faceted. The facet planes of {211} and {011} were determined from the image, and these are typical for W [20]. In some cases, the facet plane was parallel to the longer direction of the precipitate (Fig. 7b).

This study did not observe the effect of the pre-existing dislocation lines on the microstructural evolution by irradiation. Moreover, although extensive dislocation networks were present in the polycrystalline foils before irradiation, because of the rolling during the manufacture of the material, dislocation lines were not

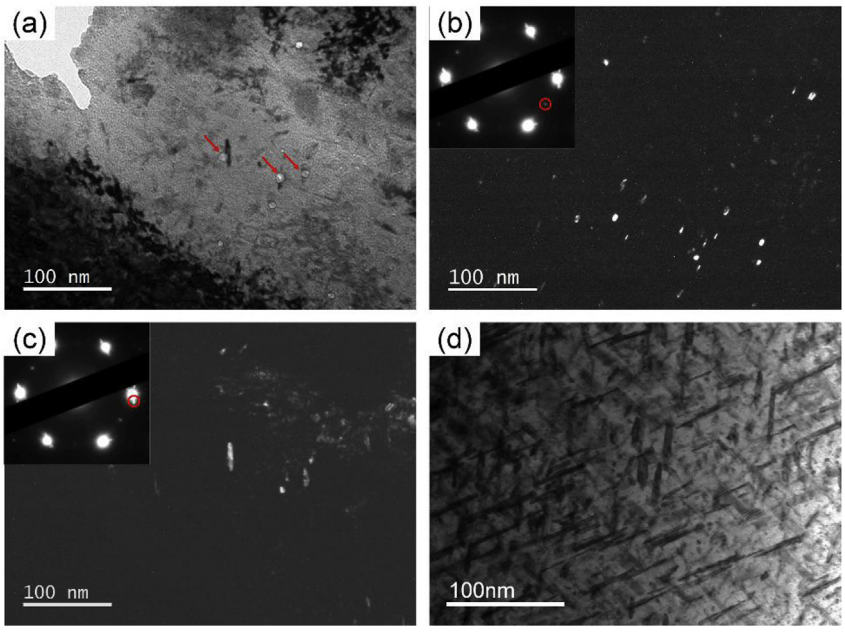

Fig. 3. TEM micrographs of single-crystal tungsten irradiated at 770 °C to 2.88 dpa. (a) BF image and (b and c) DF images taken using a diffraction spot indicated in the inserted diffraction pattern, and (d) STEM BF image. The images (a, b, c) were taken from same location. Arrows in (a) indicate voids. All the images were taken from an approximate [−111] direction.

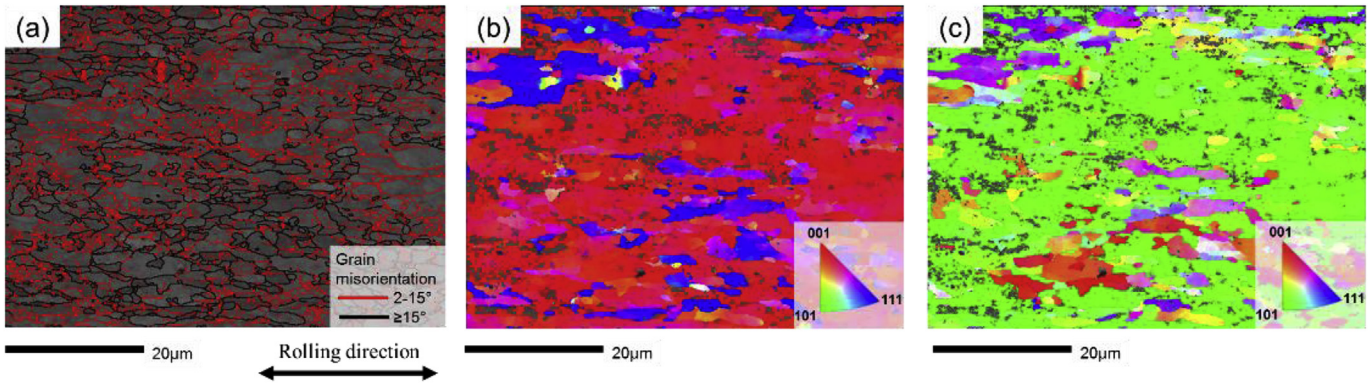

Fig. 4. EBSD analysis of unirradiated polycrystalline tungsten: (a) layered band contrast image and grain misorientation map, (b) surface normal-projected map, and (c) surface plane horizontal-projected inverse pole figure orientation map.

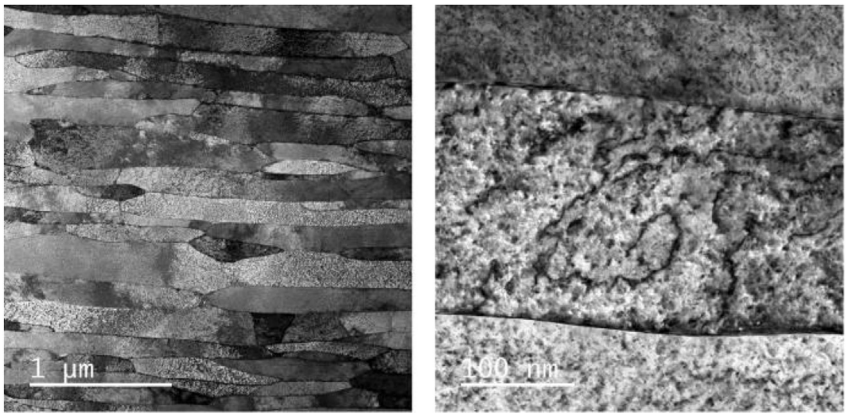

Fig. 5. STEM BF micrographs of unirradiated tungsten foil. The vertical direction in the images corresponds to the foil thickness direction.

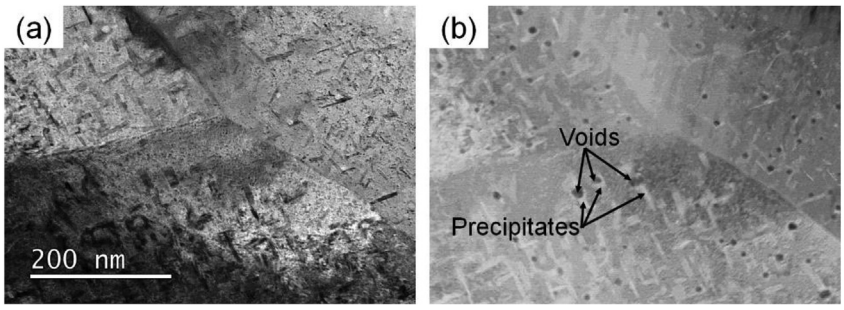

Fig. 6. STEM-BF (a) and STEM-HAADF (b) micrographs of polycrystalline tungsten neutron-irradiated at 650 °C to 2.4 dpa.

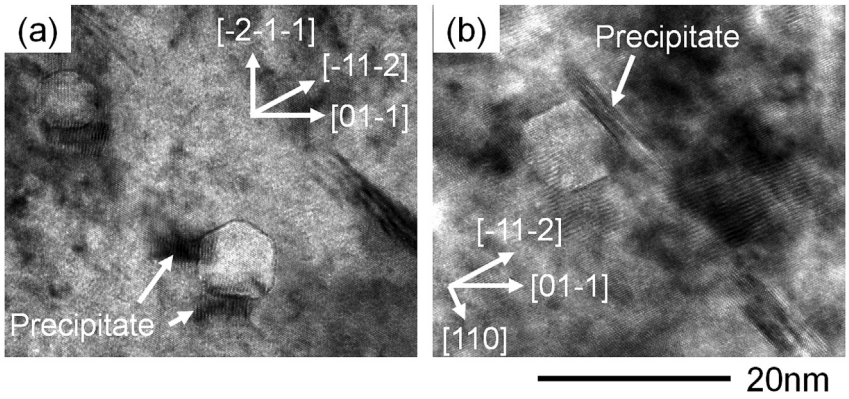

Fig. 7. (a, b) TEM BF micrograph of tungsten neutron-irradiated at 650 °C to 2.4 dpa. The images were taken from an approximate [−111] direction.

found following irradiation.

STEM EDS mapping (Fig. 8) revealed that there were large, ~100 nm–scale Re- and Os -rich phases located at the grain boundaries, but the STEM EDS mapping was unable to distinguish the smaller, ~10 nm–scale precipitates, as seen in Figs. 6 and 7. The sizes and densities of the precipitates were larger following irradiation at 500 °C to 4.6 dpa (Fig. 8b) than in Fig. 8a.

TEM DF imaging is an additional method used for observation of precipitates at grain boundaries. The DF micrograph, taken using a diffraction spot originating in the precipitate, is shown in Fig. 9. Comparing the BF and DF images, it is obvious that some of the matrix precipitates were located near the grain boundary. It is not

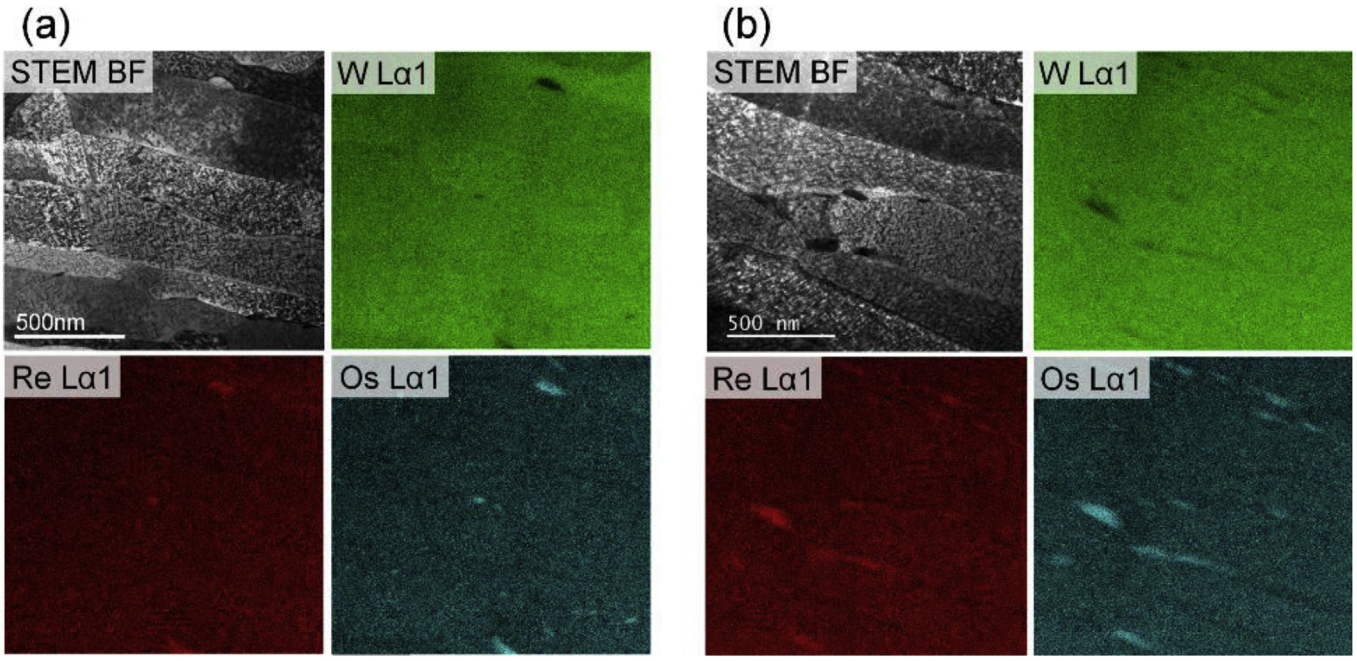

Fig. 8. STEM EDS maps of polycrystalline tungsten neutron-irradiated at (a) 650 °C to 2.4 dpa and at (b) 500 °C to 4.6 dpa.

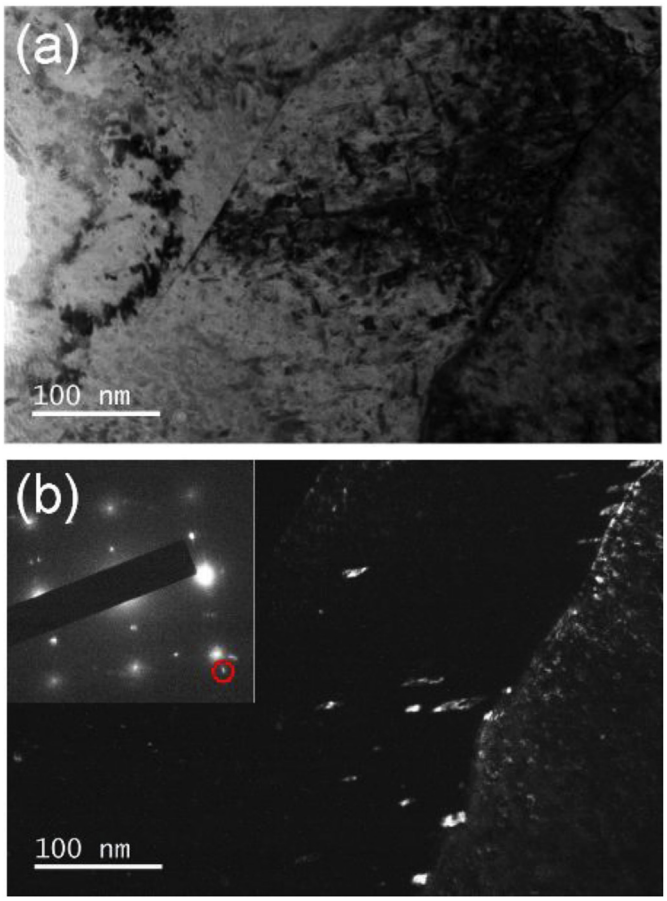

Fig. 9. TEM micrographs of polycrystalline tungsten neutron irradiated at 650 °C to 2.4 dpa: (a) BF image and (b) DF image taken using the diffraction spot indicated in an inserted diffraction pattern. Note that images (a) and (b) were taken from the same location.

clear whether the precipitates were connected with the grain boundary or not; however, Fig. 9 shows possible interaction between the grain boundary and precipitates within the W grain.

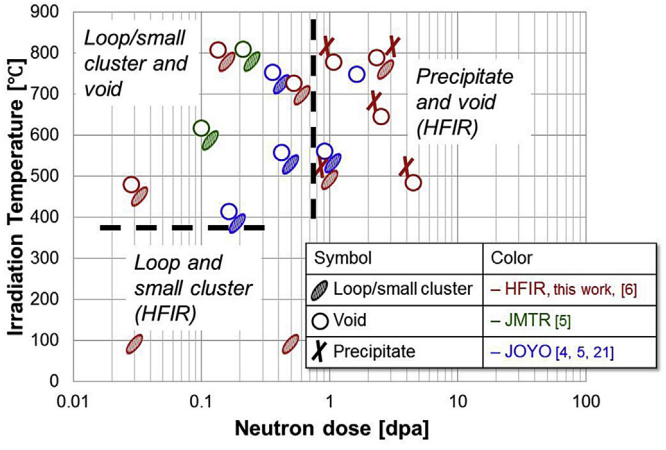

Fig. 10. Microstructural evolution in single-crystalline and polycrystalline pure tungsten materials irradiated with neutrons in this study are compared with previous results from Refs. [4–6,21].

4. Discussion

Fig. 10 summarizes the dose and temperature dependence of the microstructural evolution of pure W irradiated at different neutron energy spectra. This map has been expanded from the microstructural map originally reported by Hasegawa et al., who evaluated polycrystalline pure W irradiated in the HFIR and the Japan Materials Testing Reactor (JMTR) with a mixed spectrum, and in the fast reactor JOYO [5]. There are two boundary conditions that characterize the microstructure. The first one is the irradiation temperature of ~400 °C. Above this temperature, irradiation with both mixed and fast spectra produced voids in addition to loops and small defect clusters. This result is consistent with results from the annealing study of irradiated W by Hu et al. showing that monovacancies were effectively mobile from ~350 °C [16]. The accurate lower-temperature boundary for void formation is not available at this point owing to the lack of data for temperatures between ~90 and 400 °C. Voids were previously observed even at the very low neutron fluence of 0.17 dpa [4], and this study also found voids at only 0.03 dpa (Fig. 2a and b). An exceptional result was reported by Fukuda et al.; they did not find voids in pure W following HFIR irradiation at 500 °C to ~1 dpa [6]. The reason for this inconsistency is not clear. One possibility is that the actual irradiation temperature in that previous work was lower than the nominal value of 500 °C, since no description of the temperature measurement was present.

The second boundary condition is a neutron dose of ~1 dpa. At this dose and higher doses, precipitates are visible by TEM in both single-crystal and polycrystalline W after HFIR irradiation. In this relatively high-dose regime, void and precipitates were observed. In contrast, the fast-spectrum (JOYO) irradiation did not produce precipitates at up to 1.54 dpa; instead, a void lattice structure appeared at ~1 dpa for temperatures of 600–800 °C [5]. The result suggests that transmutation occurs at a slower rate in a fast reactor; hence, the transmutation products required to produce precipitates were not available to facilitate precipitation. Therefore, at higher neutron doses, the different neutron spectra strongly affected the microstructural development of pure W, as was also reported in the previous study [8]. The effects of the different neutron spectra on the sizes and densities of the loops and voids were discussed in the previous work [8]. The defect type for single-crystal and polycrystalline W was the same, except for the precipitation at grain boundaries in the polycrystalline W. Microstructural data for W neutron-irradiated at low temperatures to high doses have not been analyzed yet, but information from this quadrant of the parameter space may be useful for understanding the temperature-dependent precipitation behavior.

The formation of larger defect clusters is affected by the mobility of individual interstitials and vacancies. A simulation study by Derlet et al. shows that tungsten self-interstitial atoms (SIAs) move along the <111> direction with a migration energy of 0.013 eV and change direction with a rotation energy of 0.38 eV [22]. Experimental data show that the vacancy migration energy in W is 1.7 eV [23] or 2.02 eV [24]. Therefore, SIAs are highly mobile at low temperatures, and vacancies are expected to be effectively mobile at least by the void formation temperature of ~400 °C. Regarding the mobility of the transmutation elements, they are considered to effectively move under radiation via the interstitial mechanism rather than the vacancy mechanism; and the migration energies of isolated Re and Os interstitials are reported to be 0.12 and 0.31 eV, respectively, along the <111> direction [25]. These values are much smaller than the vacancy migration energy. However, the underlying mechanism of defect evolution in irradiated W is complex. In the case in which Re-W and Os-W mixed dumbbell complexes are formed, the complexes are expected to move faster via continuous

rotation with relatively small rotation energies of 0.03 and 0.16 eV, respectively [25,26]. One question is that of the impacts of interactions among SIAs, vacancies, and solutes on the precipitation process. Precipitation may be possible without displacement damage in pure W once the transmutation elements are produced by neutrons, depending on the thermal driving force and the amount and the element of transmutation. Williams et al. confirm no precipitation in a W-3 wt % Re alloy following aging at 1350 °C for 10,000 h, using electron microscope analysis and x-ray diffraction, but they found precipitates following fast-neutron irradiation at 900 °C [3]. Therefore, irradiation appeared to cause or accelerate precipitation. Recent work by Xu et al., using atom probe tomography, found W-Re nano-size clusters in a W-~2 wt % Re alloy self–ion-irradiated at low temperatures of 300 and 500 °C to 33 dpa [27]; their presence indicates possible precipitation in W with a low alloying concentration at low temperatures under irradiation. In the present work, we found relatively larger precipitates above ~1 dpa with 5–10 at. % Re and 1–5 at. % Os [6,13]. It is expected that nano-size SIA-solute clustering may be possible at lower doses, working as a precursor for the precipitates observed at higher doses.

TEM observation found that voids and precipitates appeared to be present in close proximity to each other, as shown in Figs. 6 and 7, although the two-dimensional projection of the (S)TEM images did not provide information regarding the thickness direction. Whether voids are touching the precipitates or not might affect the interpretation of the precipitation mechanism. The association of voids and precipitates, as well as the underlying mechanisms, will be discussed further in another publication.

This study found Re- and Os-rich precipitates along grain boundaries in pure W for the first time, although grain boundary precipitation has been reported in neutron-irradiated W-Re alloys with limited Os production [3,28]. Since Os is a transmutation product of Re, diffusion of Os to grain boundaries may not be essential to form Re- and Os-rich precipitates. In other words, diffusion of Re to grain boundaries is sufficient to form that type of precipitate. The migration of Re in irradiated W is expected to be faster than that of Os, based on kinetic Monte Carlo simulations [25]. He et al. found grain boundary precipitates in a W-Re alloy irradiated in the JMTR at 800 °C to 0.15 dpa, in which the matrix precipitates were absent [28]. Precipitation formed at such a low dose with a limited amount of Os indicates that grain boundary precipitation is possible with only Re. If the sink strength of grain boundaries for Re and Os is sufficient, the grain boundaries will affect the matrix precipitation. However, no denuded zone of precipitates was observed near the grain boundaries. Moreover, the matrix precipitates were formed close to the grain boundaries, as shown in Fig. 9, indicating that the effect of grain boundaries on matrix precipitation is minimal under the conditions investigated. The preliminary analysis of this study revealed that the precipitate is a coherent structure of W. The detailed chemical and structural analysis will be reported in a separate paper. The grain boundary is also a sink for interstitials and vacancies. This study observed a limited denuded zone of voids near grain boundaries, as shown in Fig. 6. He et al. also addressed that grain boundaries did not affect the void distribution in pure W irradiated at 600 °C to 0.15 dpa [28]. On the other hand, they found an ~200 nm denuded zone of dislocation loops. This result explains the absence of dislocation loops in polycrystalline W with a grain width of 200–300 nm in this study. It means the microstructure of W with larger grains is expected to be different from that observed in this study.

The observed defect types in neutron-irradiated pure W are clearly different from those in ion-irradiated pure W. Void formation was not observed in pure W following self-ion irradiation at temperatures ranging from 300 to 750 °C at doses ranging from 0.4 to 30 dpa [19]. A simulation study by Gilbert et al. [29] showed that there was a critical defect size below which vacancy loops become more energetically unfavorable than voids. A significant difference between neutron and ion irradiation is the displacement damage rate: ~1×10^{-7} dpa/s for neutrons and 3×10^{-4} dpa/s for ions [19]. There may be more time for vacancy agglomeration under neutron irradiation. Another possible explanation of the different vacancy defects is that they are due to gas impurities such as helium and hydrogen as transmutation elements, which may stabilize vacancies. Ab initio calculations revealed binding energies of 4.57 eV between helium and W vacancies, and of 1.22 eV between hydrogen and W vacancies [30]. A transmutation calculation showed helium and hydrogen production of 0.12 and 0.17 appm, respectively, in W irradiated at 19.5 dpa in the HFIR [31].

5. Conclusion

This study observed the microstructures of single-crystal and polycrystalline pure W neutron-irradiated at ~90–800 °C to 0.03–4.6 dpa in the HFIR. Small defect clusters and loops were the dominant radiation defects at ~90 °C. Both loops and voids were observed at temperatures above 460 °C to doses below ~1 dpa. Beyond a neutron dose of ~1 dpa, the precipitates attributed to transmutation elements of Re and Os were the dominant defects, in addition to voids. This study found Re- and Os-rich precipitates along the grain boundaries following irradiation to 2.4 and 4.6 dpa, showing the importance of considering grain boundary effects on precipitate evolution. The microstructures of irradiated W are highly dependent on the neutron spectrum, especially at higher neutron doses, because of the transmutation caused by thermal energy neutrons.

Acknowledgments

This work was supported by the Office of Fusion Energy Sciences, U.S. Department of Energy, under contract DE-AC05-00OR22725 with UT-Battelle, LLC, and the U.S./Japan PHENIX project on fusion research and development. A portion of this research used resources at the HFIR, a Department of Energy Office of Science User Facility operated by the ORNL. The authors would like to thank Dr. J. Reiser at Karlsruhe Institute of Technology, Germany, for providing W foil material. The authors are grateful to Dr. P. D. Edmondson at Oak Ridge National Laboratory for his valuable comments.

References

[1] S. Wurster, N. Baluc, M. Battabyal, T. Crosby, J. Du, C. García-Rosales, A. Hasegawa, A. Hoffmann, A. Kimura, H. Kurishita, Recent progress in R&D on tungsten alloys for divertor structural and plasma facing materials, J. Nucl. Mater. 442 (1) (2013) S181–S189.
[2] M. Rieth, S. Dudarev, S.G. De Vicente, J. Aktaa, T. Ahlgren, S. Antusch, D. Armstrong, M. Balden, N. Baluc, M.-F. Barthe, Recent progress in research on tungsten materials for nuclear fusion applications in Europe, J. Nucl. Mater. 432 (1) (2013) 482–500.
[3] R. Williams, F. Wiffen, J. Bentley, J. Stiegler, Irradiation induced precipitation in tungsten based, W-Re alloys, Metall. Mater. Trans. A 14 (3) (1983) 655–666.
[4] T. Tanno, M. Fukuda, S. Nogami, A. Hasegawa, Microstructure development in neutron irradiated tungsten alloys, Mater. Trans. 52 (7) (2011) 1447–1451.
[5] A. Hasegawa, M. Fukuda, S. Nogami, K. Yabuuchi, Neutron irradiation effects on tungsten materials, Fusion Eng. Des. 89 (7) (2014) 1568–1572.
[6] M. Fukuda, K. Yabuuchi, S. Nogami, A. Hasegawa, T. Tanaka, Microstructural development of tungsten and tungsten–rhenium alloys due to neutron irradiation in HFIR, J. Nucl. Mater. 455 (1) (2014) 460–463.
[7] A. Hasegawa, M. Fukuda, K. Yabuuchi, S. Nogami, Neutron irradiation effects on the microstructural development of tungsten and tungsten alloys, J. Nucl. Mater. 471 (2016) 175–183.
[8] M. Fukuda, N.K. Kumar, T. Koyanagi, L.M. Garrison, L.L. Snead, Y. Katoh, A. Hasegawa, Neutron energy spectrum influence on irradiation hardening and microstructural development of tungsten, J. Nucl. Mater. 479 (2016)

249–254.
[9] X. Hu, T. Koyanagi, M. Fukuda, N.K. Kumar, L.L. Snead, B.D. Wirth, Y. Katoh, Irradiation hardening of pure tungsten exposed to neutron irradiation, J. Nucl. Mater. 480 (2016) 235–243.
[10] T. Noda, M. Fujita, M. Okada, Transmutation and induced radioactivity of W in the armor and first wall of fusion reactors, J. Nucl. Mater. 258 (1998) 934–939.
[11] V. Sikka, J. Moteff, Identification of α-Mn crystal structure in neutron irradiated W-Re alloy, Metall. Mater. Trans. B 5 (6) (1974) 1514–1517.
[12] Y. Nemoto, A. Hasegawa, M. Satou, K. Abe, Microstructural development of neutron irradiated W–Re alloys, J. Nucl. Mater. 283 (2000) 1144–1147.
[13] L. Greenwood, F. Garner, Transmutation of MO, Re, W, Hf, and V in various irradiation test facilities and STARFIRE, J. Nucl. Mater. 212 (1994) 635–639.
[14] C. Forty, G. Butterworth, J.-C. Sublet, Burnup of some refractory metals in a fusion neutron spectrum, J. Nucl. Mater. 212 (1994) 640–643.
[15] J. Reiser, M. Rieth, B. Dafferner, A. Hoffmann, X. Yi, D.E. Armstrong, Tungsten foil laminate for structural divertor applications–Analyses and characterisation of tungsten foil, J. Nucl. Mater. 424 (1) (2012) 197–203.
[16] X. Hu, T. Koyanagi, M. Fukuda, Y. Katoh, L.L. Snead, B.D. Wirth, Defect evolution in single crystalline tungsten following low temperature and low dose neutron irradiation, J. Nucl. Mater. 470 (2016) 278–289.
[17] A.A. Campbell, W.D. Porter, Y. Katoh, L.L. Snead, Method for analyzing passive silicon carbide thermometry with a continuous dilatometer to determine irradiation temperature, Nucl. Instrum. Methods Phys. Res. Sect. B Beam Interact. Mater. Atoms 370 (2016) 49–58.
[18] V. De Castro, T. Leguey, M.A. Auger, S. Lozano-Perez, M. Jenkins, Analytical characterization of secondary phases and void distributions in an ultrafine-grained ODS Fe–14Cr model alloy, J. Nucl. Mater. 417 (1) (2011) 217–220.
[19] X. Yi, M.L. Jenkins, K. Hattar, P.D. Edmondson, S.G. Roberts, Characterisation of radiation damage in W and W-based alloys from 2MeV self-ion near-bulk implantations, Acta Mater. 92 (2015) 163–177.
[20] P. Goodhew, Shapes of pores in metals, Metal Sci. 15 (9) (1981) 377–385.
[21] M. Fukuda, T. Tanno, S. Nogami, A. Hasegawa, Effects of Re content and fabrication process on microstructural changes and hardening in neutron irradiated tungsten, Mater. Trans. 53 (12) (2012) 2145–2150.
[22] P.M. Derlet, D. Nguyen-Manh, S. Dudarev, Multiscale modeling of crowdion and vacancy defects in body-centered-cubic transition metals, Phys. Rev. B 76 (5) (2007) 054107.
[23] R. Balluffi, Vacancy defect mobilities and binding energies obtained from annealing studies, J. Nucl. Mater. 69 (1978) 240–263.
[24] J. Mundy, S. Ockers, L. Smedskjaer, Vacancy migration enthalpy in tungsten at high temperatures, Philos. Mag. A 56 (6) (1987) 851–860.
[25] T. Suzudo, M. Yamaguchi, A. Hasegawa, Migration of rhenium and osmium interstitials in tungsten, J. Nucl. Mater. 467 (2015) 418–423.
[26] T. Suzudo, M. Yamaguchi, A. Hasegawa, Stability and mobility of rhenium and osmium in tungsten: first principles study, Model. Simul. Mater. Sci. Eng. 22 (7) (2014) 075006.
[27] A. Xu, D.E. Armstrong, C. Beck, M.P. Moody, G.D. Smith, P.A. Bagot, S.G. Roberts, Ion-irradiation induced clustering in W-Re-Ta, W-Re and W-Ta alloys: an atom probe tomography and nanoindentation study, Acta Mater. 124 (2017) 71–78.
[28] J. He, G. Tang, A. Hasegawa, K. Abe, Microstructural development and irradiation hardening of W and W–(3–26) wt% Re alloys after high-temperature neutron irradiation to 0.15 dpa, Nucl. fusion 46 (11) (2006) 877.
[29] M. Gilbert, S. Dudarev, P. Derlet, D. Pettifor, Structure and metastability of mesoscopic vacancy and interstitial loop defects in iron and tungsten, J. Phys. Condens. Matter 20 (34) (2008) 345214.
[30] C.S. Becquart, C. Domain, U. Sarkar, A. Debacker, M. Hou, Microstructural evolution of irradiated tungsten: Ab initio parameterisation of an OKMC model, J. Nucl. Mater. 403 (1) (2010) 75–88.
[31] M. Sawan, Transmutation of tungsten in fusion and fission nuclear environments, Fusion Sci. Technol. 66 (1) (2014) 272–277.